Applied Clay Science 250 (2024) 107300

Contents lists available at ScienceDirect

Applied Clay Science

journal homepage: www.elsevier.com/locate/clay

Research Paper

Sebacate intercalated Ca—Al layered double hydroxide pigments for corrosion protection of low carbon steel: Anion exchange and electrochemical properties

Andrea Cristoforetti [a,*], Federico Parola [a], Francesco Parrino [a], Javier Izquierdo [b], Ricardo M. Souto [b], Stefano Rossi [a], Flavio Deflorian [a], Michele Fedel [a]

[a] Department of Industrial Engineering, University of Trento, via Sommarive n. 9, 38123 Trento, Italy
[b] Institute of Material Science and Nanotechnology, P.O. Box 456, University of La Laguna, E-38207 La Laguna, Tenerife, Canary Islands, Spain

ARTICLE INFO

Keywords:
Corrosion protection
Corrosion inhibition
Layered double hydroxides
Hydrotalcite
Carboxylates
Anion exchange

ABSTRACT

Sebacate (SB) molecules were incorporated into Ca—Al layered double hydroxides (CaAL-LDH) using a hydrothermal method. The resulting products underwent characterization through X-ray diffraction, infrared spectroscopy, and scanning electron microscopy. To investigate the release kinetics and thermodynamics of the corrosion inhibitor, total organic carbon analysis (TOC) was employed. A comparison was made with CaAl-LDH prepared without corrosion inhibitors, in which nitrates were the primary anions within the layered clay structure. An assessment of anion exchange between nitrates and chlorides was conducted using total nitrogen analysis (TN). The SB anion comprised approximately 49.2% of the total dried powder synthesized, with a maximum release efficiency of around 86.7% fitting a Langmuir model. For the evaluation of the corrosion inhibition effect on steel surfaces, electrochemical impedance spectroscopy, potentiodynamic polarization, and scanning vibrating electrode technique were employed. The corrosion inhibition impact was ascribed to the liberation of SB anions from the CaAl-LDH pigments, accompanied by alkalinization stemming from partial particle dissolution. Additionally, the incorporation of organic molecules notably enhanced the stability of pigments in aqueous solutions compared to similar ones hosting nitrates. These findings suggested that CaAl-LDH pigments have potential as nanocontainers for organic inhibitors, showing promising prospects in the field of corrosion research.

1. Introduction

Organic coatings are commonly used to protect steel substrates against corrosion, keeping the structures' mechanical and functional properties unaltered (Grundmeier et al., 2000; Lyon et al., 2017; Pélissier and Thierry, 2020; Trentin et al., 2022). To assure a given service life, generally, the organic coatings have to provide (i) adhesion to the substrate, (ii) ions/water barrier properties, and (iii) corrosion inhibition. Several inhibitive particles and conversion coatings have been explored over the years to improve the durability of substrates. Environmental and human health-related issues strongly limit the use of many traditional chemicals, as the most successful conversion treatments contain chromium (VI) and other highly toxic compounds (Bastos et al., 2006; Milošev and Frankel, 2018; Cristoforetti et al., 2021). In the last decades, the most adopted inhibitors on steel were based on chromates such as strontium chromate (Prosek and Thierry, 2004), but also non-toxic substances like zinc phosphate (Mahdavian and Attar, 2005; Alibakhshi et al., 2014) and micaceous iron oxide (Forsgren, 1996; Kalenda et al., 2004) have been widely studied. The use of environmentally friendly inhibitors has become essential in recent years (Sinko, 2001; Indumathi et al., 2011; Bi et al., 2014; Dodds et al., 2017). For instance, molecules containing carboxylic groups are demonstrated to form complexes with iron ions to compete effectively with chloride ions (Saurbier et al., 1994; Lahem et al., 2012). Based on this property, acid organic molecules are shown to protect steel, copper, and aluminum alloys in near-neutral solutions (Hefter et al., 1997; Rocca and Steinmetz, 2001; Rammelt et al., 2008). The precise mechanism of corrosion mitigation by carboxylates and dicarboxylates is not entirely known, but

* Corresponding author.
E-mail addresses: andrea.cristoforetti@unitn.it (A. Cristoforetti), fedeico.parola@studenti.unitn.it (F. Parola), francesco.parrino@unitn.it (F. Parrino), jizquier@ull.edu.es (J. Izquierdo), rsouto@ull.es (R.M. Souto), stefano.rossi@unitn.it (S. Rossi), flavio.deflorian@unitn.it (F. Deflorian), michele.fedel@unitn.it (M. Fedel).

https://doi.org/10.1016/j.clay.2024.107300
Received 9 October 2023; Received in revised form 9 February 2024; Accepted 14 February 2024
Available online 17 February 2024

some studies highlighted the crucial role of the hydrophobic character of the thin layer developed upon interaction with the metal substrate (Shulman and Bauman, 1995; Rocca and Steinmetz, 2001; Georges et al., 2008; Boisier et al., 2009). In fact, the main factor influencing the efficiency of the carboxylates is their chain length (Hefter et al., 1997; Lahem et al., 2012). Concerning dicarboxylates, their behavior ranges from corrosive for short-chain structures ($3 < n$) to protective for longer ones ($3 \leq n \leq 8$). Both mono- and di-carboxylates present a critical length ($n = 11$ and 13, respectively) over which the inhibition effect dramatically drops due to micelle formation.

Given the proven efficacy for steel of sodium salts of various organic acids, such as adipic or sebacic acid (Godinez-Alvarez et al., 2004; Rammelt et al., 2008, 2011; Caballero et al., 2022; Guo et al., 2022), the question arises of a technological solution to tailor the release and activation of the inhibitor when necessary. Although they can be incorporated directly into the organic coating with the appropriate amount of additives, in this way, there will be no control over the release of the dicarboxylates.

For this reason, layered double hydroxide (LDH) anionic clays, also known as hydrotalcite, are one of the most promising systems, both applicable as a treatment of metal surfaces before the painting stage and as a pigment embedded in an organic coating (Williams, 2010; Williams and McMurray, 2012; Zheludkevich et al., 2012; Nguyen et al., 2018; Fedel and Zampiccoli, 2021; Fedel et al., 2021; Wint et al., 2021; Cao et al., 2022; Fedel et al., 2024). LDH consists of a mixture of lamellar hydroxides organized in a layered structure able to host anions or negatively charged molecules. This system displays an anion-exchange character and is therefore suitable as an anionic inhibitor nanocontainer (Newman and Jones, 1998; Millange et al., 2000; Mahajanam and Buchheit, 2008; Poznyak et al., 2009; Zheludkevich et al., 2010, 2012; Li et al., 2011; Stimpfling et al., 2014; Grigoriev, 2015; Nguyen et al., 2018). In a typical LDH structure, atoms are organized following the general formula (1) where M^{2+} and M^{3+} are metal ions, A^{n-} represents the exchangeable anion and the value of x varies from 0.25 to 0.33 (Miyata, 1983; Drits et al., 1987). The presence of the trivalent cations determines an excess of positive charge in the structure, which causes the intercalation of the anions. The M^{2+}/M^{3+} ratio, tunable during the synthesis, determines the concentration of the intercalated A^{n-} particles.

$$\left[M^{2+}{}_{x-1}\, M^{3+}{}_{x}\, (\mathrm{OHOH})_2\right]^{x+} \left[A^{n-}{}_{x/n}\, y\mathrm{H_2O}\right] \quad (1)$$

Several metal cations have been widely employed in pigment production; ZnAl and MgAl are the most popular pigment systems (Mahajanam and Buchheit, 2008; Tedim et al., 2012; Williams and McMurray, 2012; Mei et al., 2019; Wint et al., 2021; Li et al., 2023), but other elements are worth studying. ZnCr, LiAl, and CaAl are other examples in the literature related to very different research fields, from medicine to corrosion science (Meyn et al., 1990; Poznyak et al., 2009). Besides the capability to host and release inhibitor compounds, LDH pigments based on hydrotalcite or calcined hydrotalcite may be capable of acting as chloride scavengers since Cl^- results favored in the anion exchange with respect to organic molecules (thanks to its smaller size) (Miyata, 1983; Meyn et al., 1990; Kameda et al., 2000; Chen et al., 2015; Bouali et al., 2020). Based on this ability, LDH structures can be tailored by intercalating specific corrosion inhibitor molecules into their lamellar frames, and these could be used as a reservoir that is activated only when needed. The application interest in combining organic acids with hydrotalcite lies in the health safety and environmental and economic advantages of the production, use, and disposal of such compounds.

This work aimed to develop pigments based on the CaAl-LDH structure capable of mitigating the onset and development of corrosion of organic-coated steel surfaces. The synthesized particulate material was specifically formulated and analyzed in the pigmentary form, intended for incorporation into paint formulations. Taking advantage of the anion exchange ability of the layered double hydroxide compounds, an environmentally friendly organic corrosion inhibitor such as disodium SB was intercalated during pigment synthesis, and its ability to be released and improve the corrosion resistance of steel was investigated. Furthermore, the substitution of the most common zinc and magnesium with the less investigated combination with calcium could give an additional appeal for the low cost of the raw materials needed for the synthesis. The morphology, composition, and structure of the pigments were characterized by X-ray powder diffraction (XRD), Fourier-transform infrared spectroscopy (FTIR), and scanning electron microscopy (SEM). Since the majority of publications present in the literature lacked fundamental information on the actual amount of SB intercalated and absorbed on the hydrotalcite-like particles, this paper tries to provide more precise data to make different studies comparable. The concentration of SB in the pigments and the ion-exchange properties of disodium sebacate were studied using TOC and TN analysis. Electrochemical activity related to corrosion protection was investigated using electrochemical impedance spectroscopy (EIS), potentiodynamic polarization curves (PDP), and scanning vibrating electrode technique (SVET) on bare steel in contact with a dilute saline solution containing the studied particles. Based on the obtained data, the potential of CaAl-LDH intercalated with an organic corrosion inhibitor was discussed. This study could contribute to the development of such innovative systems for corrosion protection of metallic structures, whose great strength lies in cost efficiency, safe handling of production waste, and disposal.

2. Experimental

2.1. Pigment synthesis

CaAl-LDH was synthesized by dissolving 6.25 g of NaOH and 9.10 g of $NaNO_3$ in 44 mL of demineralized water, and under constant nitrogen bubbling, 80 mL of a second solution containing 17 g of $Ca(NO_3)_2 \cdot 4H_2O$ and 11.70 g of $Al(NO_3)_3 \cdot 9H_2O$ was added dropwise. The aqueous mixture of the salts (with pH 10.5 at room temperature) was kept in a sealed three-neck flask at 80 °C for 24 h under magnetic stirring conditions. Then, the obtained suspension was collected and centrifuged 4 times at 4500 rpm for 2 min to separate the solid content, which was washed with fresh demineralized water each time. Additionally, the solid powder was washed 2 times using acetone in the same rotary setting. The product was finally dried in an oven at 40 °C for 24 h and milled to obtain a white powder (Saha et al., 2018). About 5.7 g of dried powder was produced in each synthesis.

In the case of the production of the CaAl-LDH pigments loaded with disodium sebacate (named LDH/SB), the synthesis procedure was modified to intercalate and adsorb it in the lamellar structure of the hydrotalcite-like matter. In particular, the $NaNO_3$ was replaced by 7 g of disodium sebacate (supplied by Merck, Darmstadt, Germany). The rest of the experimental procedure resembled the synthesis described above.

To test the ion exchange performances of synthesized CaAl-LDH and LDH/SB with respect to chloride anions, 3 g/L of each type of pigment were added separately to a 1 mol/L NaCl solution. Finally, the solution was kept at 25 °C and stirred for 24 h. Then the powder was washed with the same procedure adopted in the case of the production of the pristine pigment (Meyn et al., 1990).

2.2. Pigment characterization

The powdery samples were analyzed by FTIR using a VARIAN 4100-FTIR Excalibur Series (4 cm^{-1} resolution, 32 scans, 4000–500 cm^{-1} wavenumber range). The specimens were prepared in 350 mg KBr circular-pressed tablets containing 0.9 mg of sample.

Powder X-ray diffraction patterns of the pigments were obtained using an X'Pert High Score diffractometer - Rigaku, (Japan) with Cu Kα emission source ($\lambda = 1789$ Å) and the monochromator working at 30 kV and 10 mA. The product was identified referring to JCPDS #870493 for CaAl-LDH.

A Jeol (Japan) JSM-IT300 scanning electron microscopy (SEM)

equipped with an EDS detector was employed to observe the morphology of the LDH powder structure.

A TOC-TN analysis carried out by means of a Shimadzu (Japan) TOC-L apparatus was performed to study the kinetics and thermodynamics of the anion exchange process. The pigments were added in the concentration of 3 g/L to five different solutions of sodium chloride, namely 0.5, 0.1, 0.05, 0.01, and 0 mol/L (blank, chloride-free) solution. TOC measurements were performed periodically during 48 h of magnetic stirring at room temperature after filtration. The organic carbon concentration was determined by subtracting the total carbon and the inorganic portion in the solution. Similarly, TN analysis was performed for 48 h at different initial chloride concentrations from 0.0001 mol/L to 0.5 M. The amount of SB loaded in LDH/SB pigments during synthesis was evaluated by TOC analysis in a solution containing 3 g/L of pigments that was acidified at pH 1 with HNO_3. In this acidic condition, the LDH rapidly dissolves in the solution (Jobbágy and Regazzoni, 2011; Gomes et al., 2020). Employing the TN analysis, a similar procedure was adopted to evaluate the amount of nitrates in the LDH pigments, this time by lowering the pH to 1 using a controlled addition of a 1 mol/L HCl solution.

EIS and PDP were performed on pickled (15 min in 2 mol/L HCl) bare steel surfaces with a 0.05 mol/L NaCl solution in which the different pigments were added in a 3 g/L concentration. Autolab 302 N potentiostat/galvanostat/FRA (Metrohm AG, Switzerland) was used in a three-electrode configuration, where the steel panel acted as the working electrode. Platinum and Ag/AgCl/3.5 mol/L KCl electrodes were chosen as the counter and the reference electrodes, respectively. EIS spectra were recorded over the 0.01 Hz - 100 kHz range with a signal amplitude of 5 mV (RMS, root mean square) and 6 points per decade after 2 h of immersion. EIS results were analyzed in terms of equivalent electric circuits using ZSIMPWIN® software. PDP were collected at a scan rate of 0.2 mV/s polarizing from −0.050 V to +0.700 V vs. the OCP value after a wait time of 3 h. In the electrochemical investigation, commercial disodium sebacate was also considered as a free-standing pigment to compare it to the particles listed above and to distinguish between the contributing effects of the various compounds.

SVET measurements were performed by a system from Applicable Electronics (Forestdale, MA, USA). A 20 μm platinum-black-coated tip was chosen as a probe, and the working height for scanning the samples was set at 150 μm. The vibrating amplitudes of the probe were set to 40 and 30 μm, parallel and normal to the surface, respectively. Two platinum wires acted as signal and reference electrodes. A video microscope was used to place the tip at a chosen distance and to capture images of the sampled area. A 0.01 mol/L NaCl solution was employed for the SVET measurements, and the powders under study were added in a 3 g/L concentration similar to the EIS and PDP analyses. The electrochemical activity maps were recorded over a bare steel surface of 4 × 4 mm^2 following a meandering pathway from left to right and top to bottom. The results obtained after 3 h of immersion were compared.

3. Results

3.1. Physicochemical characterization of the pigments

The hydrothermal synthesis produced a powdery matter composed of hexagonal-shaped particles (Fig. 1a) organized in multilayer stacks typical of LDH systems (Tabish et al., 2022). Considering the particles individually, the plate's envelope was of the order of 10 μm. The drying process was responsible for the disordered aggregation of piles of lamellae forming uneven clusters (Fig. 1b).

Any morphological differences were detected between the LDH and

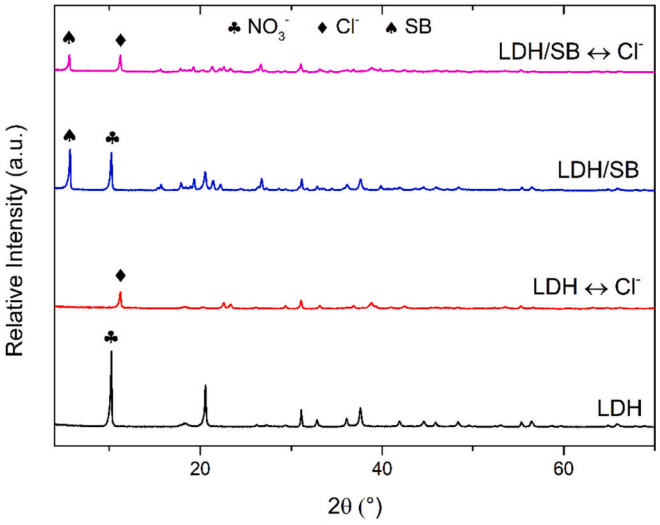

Fig. 2. XRD pattern of LDH and LDH/SB pristine powder, before and after SB-chloride and nitrate-chloride anion exchange.

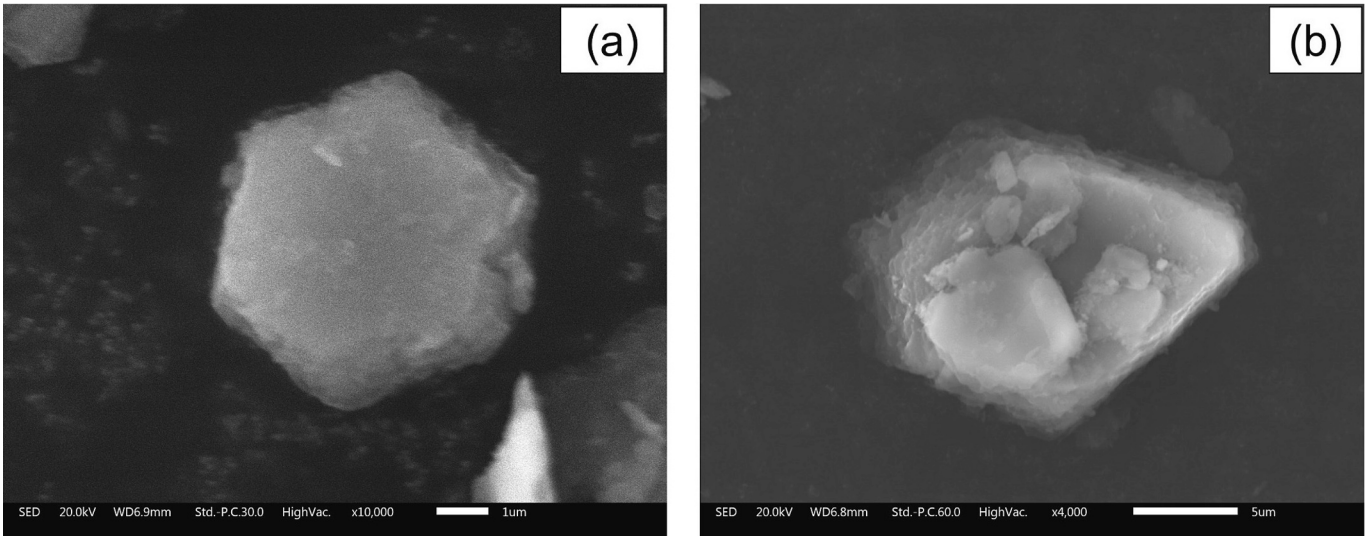

Fig. 1. SEM-SE of a single hexagonal LDH particle (a) and an example of an LDH particle cluster (b). Both images refer to pristine LDH particles without the SB addition.

LDH/SB particles by SEM analysis.

Both the XRD (Fig. 2) and the FTIR (Fig. 3a) analyses confirmed the LDH structure of the powder sample. The diffraction pattern shown in Fig. 2 presents the reflections peculiar for such systems at 10.24°, 20.58°, and 31.10° values of diffraction angles (JCPDS #870493) (Zhang et al., 2012; Szabados et al., 2016; Saha et al., 2018), corresponding respectively to (003), (006), and (012) planes (Nguyen et al., 2018).

The type of anion intercalated in the layered structure determined the distance between the lamellae, which can be calculated from the diffraction peak positions (003) employing Bragg's law (Epp, 2016). The values of interlamellar space reported in Table 1 are in agreement with the literature on CaAl-LDH (Zhang et al., 2012; De Sá et al., 2013; Szabados et al., 2016) and the marked difference in the size of the anion was highlighted in the pattern (Fig. 2). The LDH pristine powder obtained without loading any corrosion inhibitor was characterized by nitrate anions occupying the interlamellar space (Vieille et al., 2003; Radha et al., 2005; Saha et al., 2018), and it resulted in a *d*-value of 0.86 nm. Upon replacing the sodium nitrate with SB during the synthesis, the *d*-value increased, and the XRD pattern presented a marked reflection at 5.70° that was attributed to the portion of the anionic clay successfully loaded with the inhibitor molecules (LDH/SB) (Choy et al., 2008; Caballero et al., 2022), and their distance was calculated to be 1.55 nm. The original signal at 10.24° was still present in this sample, demonstrating the incomplete SB intercalation process (De Sá et al., 2013).

Fig. 2 also displays the cases where the particles were immersed for 24 h in 1 mol/L NaCl solution. Since the chloride exchange spontaneously happened both with nitrates and SB initially intercalated in the lamellae (Nguyen et al., 2018; Bouali et al., 2020), a new diffraction reflection rose in the X-ray pattern at slightly higher 2θ angle values than that related to the LDH with intercalated nitrates, entirely replacing it. From the shift of the reflections from 10.24° to 11.22°, it could be inferred a significant replacement of nitrates by chlorides, while the remaining reflection of LDH/SB at 5.70° after contact with the saline solution, despite the large stoichiometric excess of chlorides with respect the SB, testified to the partially incomplete exchange process. The reflections' intensity declined following immersion in the saline solution, indicating a reduction in crystallinity as a likely cause.

FTIR further confirmed SB intercalation in the lamellae by the presence of bands typical of the SB spectrum (Kloprogge et al., 2002; Abdolmohammad-Zadeh and Kohansal, 2012; De Sá et al., 2013) and its incomplete release (Fig. 3a), in accordance with XRD outcomes. All LDH samples reported in Fig. 3a displayed a broad band at 3475 cm^{-1} typical for the stretching vibrations of -OH groups in the brucite-like layers of the hydrotalcite-like structure and adsorbed water in the interlayer region. Angular deformation of this signal band was found at 1623 cm^{-1} with different intensities based on the type of hosted anion (Kloprogge et al., 2002; De Sá et al., 2013). The spectrum related to SB was characterized by the signals attributed to the C—H stretching at 2936 cm^{-1}, 2914 cm^{-1}, and 2848 cm^{-1} (Nguyen et al., 2018). These bands were significatively present in the sample LDH/SB, also in the case where the SB release was promoted by the contact with chloride ions as evidence of a residual presence of the organic molecules. The CaAl-LDH structure was recognizable by the characteristic Ca—O and Al—O bands at 590 cm^{-1} and 785 cm^{-1}, respectively. Fig. 3b highlights the detail of the region of the carboxyl group for SB molecules and LDH/SB pigments. Disodium sebacate laid on the hydrotalcite-like lamellae in the form of a carboxylate anion, which influences the FTIR signal of the COO^- group when it experienced different coordination (Zeleňák et al., 2007). In the spectra of LDH/SB, some intense signals were found for $\nu_{as}(COO^-)$ at 1569 cm^{-1} and 1552 cm^{-1}, and the other two attributed to $\nu_s(COO^-)$ at 1469 cm^{-1} and 1410 cm^{-1} (Czakis-Sulikowska and Czylkowska, 2004; Dolamic and Bürgi, 2006, 2007; Vargová et al., 2011; Fedel et al., 2019). The presence of two distinct coordination modes of the similar group in the LDH/SB could be explained by the availability of two possible metallic elements (Al and Ca) for interaction with the carboxylic groups (Lewandowski et al., 2005; Zeleňák et al., 2007).

In the case of carboxylic acids bonded to metal cations, the possible coordination modes are unidentate, chelating bidentate, and bridging bidentate (Lu and Miller, 2002; Van Den Brand et al., 2004). These could be discerned by the difference in the adsorption bands ($\Delta\nu = \nu_{as}(COO^-) - \nu_s(COO^-)$) (Van Den Brand et al., 2004; Fedel et al., 2019). For the interaction with Al(III) bidentate, bridging coordination was reported with signals at 1554 cm^{-1} and 1420 cm^{-1} (Lewandowski et al., 2005), which were values similar to those encountered in this case.

Table 1
Calculated (003) d-value from the XRD pattern reflections positions, variation for the intercalated anion.

h,k,l	Reflections position	*d* – value
0,0,3	(°)	(nm)
LDH – NO_3^-	10.24	0.86
LDH – Cl^-	11.22	0.79
LDH – SB	5.70	1.55

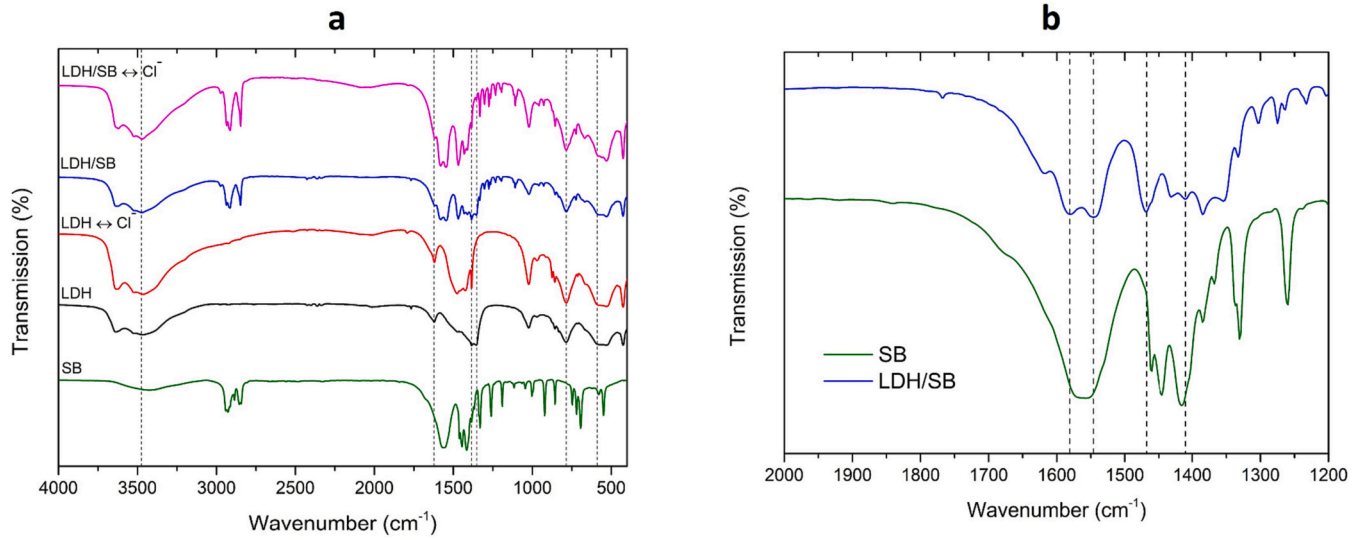

Fig. 3. FTIR - ATR spectra of LDH and LDH/SB pristine powder, before and after chlorides anion-exchange (a), and the comparison of the signal attributed to carboxylic groups stretching in the SB versus the different coordination in the LDH/SB configuration (b).

Furthermore, bidentate bridging was reported to occur when $\Delta\nu(COO^-)_{studied\ complex} < \Delta\nu(COO^-)_{sodium\ salt}$; in the case of disodium sebacate, it resulted in 146 cm^{-1}, a value in accordance with the references available in the literature (Fedel et al., 2019) and higher than the $\Delta\nu$ for Al which stood at 142 cm^{-1}. The outcome of the presented discussion on the interaction between the carboxylic group and the aluminum hydroxide was similar to the results reported by Van den Brand et al. (Van Den Brand et al., 2004). Then for Ca-bonds, $\Delta\nu$ results in 100 cm^{-1}, which lies in the range typical for the chelating bidentate binding (60–100 cm^{-1}) (Dobson and McQuillan, 1999), and it also verifies the condition: $\Delta\nu(COO^-)_{studied\ complex} << \Delta\nu(COO^-)_{sodium\ salt}$ (Lewandowski et al., 2005). Therefore, the adsorption of SB on a hydrotalcite-like system could be assumed to follow two distinct coordination modes: chelating bidentate, likely with Ca atoms, and bidentate bridging with Al. Hence an aluminum cation was supposed to interact equally with the two oxygen atoms belonging to the COO^- group, while in the bridging mode, each oxygen atom of the carboxylic group was bonded with two different calcium cations (Nara and Tanokura, 2008).

3.2. Anion release

The amount of SB present in the LDH/SB pigments was estimated to be 49.2 wt% of the synthesized powder by means of TOC measurements. This value accounted for both intercalated or adsorbed anions on the LDH structure, and it was estimated following the procedure of dissolution in an acidic solution reported in Section 2.2.

Negligible SB release was found (Fig. 4a, Blank) when the LDH/SB particles were immersed in pure water for up to 48 h, thus indicating a stabilizing effect of SB in the LDH structure. On the other hand, when chlorides were present, the particles rapidly released the inhibitor, approaching the equilibrium value within the initial hour of immersion. The kinetic evolution of anions substitution was well represented by the exponential model reported in Eq. (2). A best-fitting procedure afforded the pre-exponential term A (%), which increases in absolute value with the chloride concentration, and the apparent kinetic constant k ($hour^{-1}$). Values are reported in Table 2. The parameter A corresponds to the SB fraction released at the equilibrium. The kinetic constant k varied within a range (1.74–8.13 h^{-1}) in the same order of magnitude despite the presence of chlorides as similarly reported in affine works (Ho et al., 2000; Lazaridis and Asouhidou, 2003; Lv et al., 2006).

Table 2
SB release kinetic parameters and correlation coefficient for solutions of different chloride concentrations in contact with the LDH/SB pigments.

Fitting parameters	0.01 mol/L NaCl	0.05 mol/L NaCl	0.1 mol/L NaCl	0.5 mol/L NaCl
k ($hour^{-1}$)	2.08	1.74	6.51	8.13
A (%)	4.96	20.3	29.9	62.1
R^2	0.890	0.971	0.970	0.991

$$y = A\left(1 - e^{(-kt)}\right) \quad (2)$$

The incomplete release of SB even at the highest chloride concentration depicted in Fig. 4a was in agreement with the XRD and IR results previously described. This fact could be additionally highlighted by plotting the equilibrium values of the fraction released after 24 h at various chloride concentrations against the equilibrium values of chloride ions (Fig. 4b). The evolution followed a Langmuir-type isotherm according to the Eq. (3):

$$q_e = \frac{QK_LC_e}{1 + K_LC_e} \quad (3)$$

where Q represents the maximum capacity (%) of chloride adsorption as a monolayer, and K_L is the Langmuir adsorption constant. C_e and q_e are the equilibrium chloride concentration and the released fraction (%), respectively (Lv et al., 2006; Kokalj, 2022). This model more closely fitted the experimental data ($R^2 = 1$) with respect to the Freundlich one (Eq. (4)), in agreement with the literature of the subject (Lv et al., 2006; Xu et al., 2017; Zuo et al., 2019). The Freundlich constants K_F and n are temperature-dependent parameters related to intensity and adsorption capacity (Lv et al., 2006; Brahma and Saikia, 2022). The calculated

Table 3
Langmuir and Freundlich parameters for the chloride adsorption isotherm of LDH/SB pigments.

Model	Langmuir			Freundlich		
Fitting parameters	Q (mg/g)	K_L (L/mol)	R^2	K_F (mg/g)	n	R^2
LDH/SB	86.7	5.95	1.000	94.3	0.53	0.981

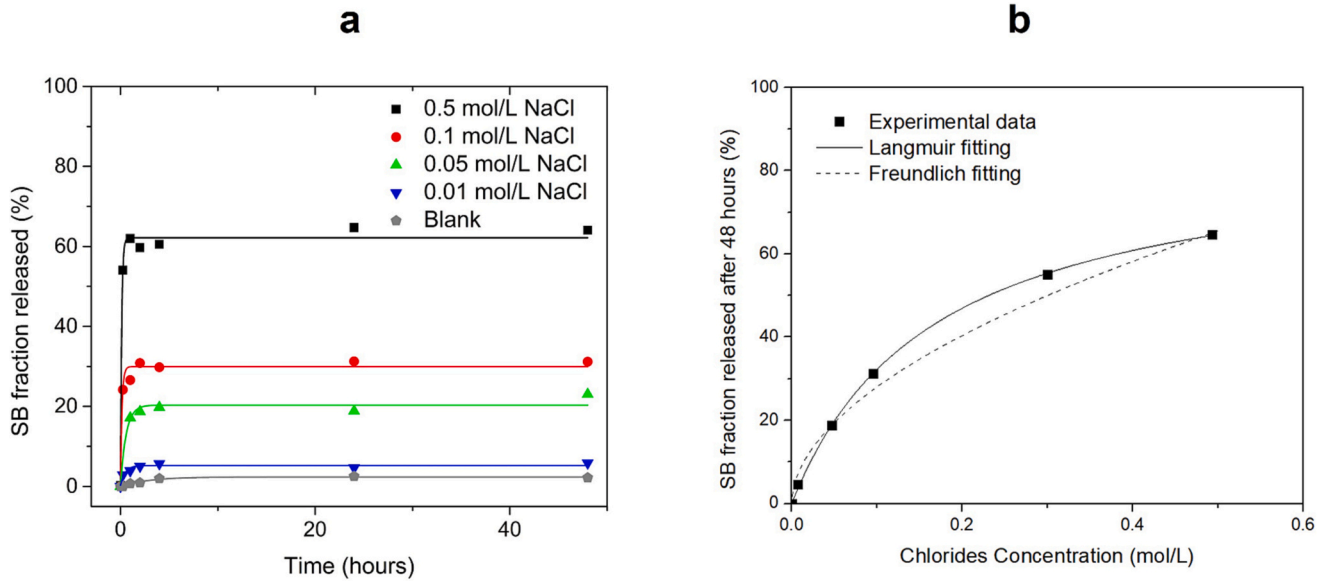

Fig. 4. SB release curves in 0.5 M, 0.1 M, 0.05 M, 0.01 mol/L NaCl, and pure water (Blank) solutions over contact time obtained from TOC analysis (a). Langmuir and Freundlich fit the equilibrium values at 24 h of SB release for various chloride concentrations at equilibrium (b).

parameters from the two considered models are listed in Table 3. The n value varied in the range of 0.1–0.5 in accordance with the values obtained in similar studies available in the literature (Lv et al., 2006; Xu et al., 2017).

$$q_e = K_F C_e^{\,n} \quad (4)$$

The reason behind the higher correlation coefficient (R^2) in the case of the Langmuir model could be justified by considering the ionic character of all the LDH adsorption sites (Zhang et al., 2022). Accordingly, one assumption of Langmuir's model was the existence of monolayer adsorption onto homogeneous sites (Wang and Guo, 2020). Finally, according to the Langmuir model, the maximum SB release capacity stood at 86.7% of the overall amount present in the synthesized particles, which corresponded to the predicted plateau of the fitting curve.

Aiming to compare the hydrotalcite-like particles loaded with SB with the reference case where only nitrates were present, a similar study based on the total nitrogen present in the testing solution upon the addition of LDH powder was carried out. The total amount of nitrates present in the synthesized particles was found to be 17.2 wt% by TN analysis after complete solubilization of the pigments in acidic solutions at pH 1 (Jobbágy and Regazzoni, 2011; Gomes et al., 2020). Fig. 5a reports the nitrate release curves for different chloride concentrations ranging from 0 ("Blank", pure water) to 0.5 mol/L NaCl. The quantity of anions liberated was initially quantified in terms of the total ppm of nitrogen, rather than assessing the portion released through anion exchange. This was because the release of NO_3^- progresses over time, even in the absence of chlorides (blank). Therefore, hydrotalcite-like matter loaded with nitrates was poorly stable in water if compared with the one loaded with SB. Notably, the low stability of nitrate-loaded LDH was in agreement with other solubility studies and was reported to strongly depend on the type of anion hosted on the structure (Allada et al., 2002; Bernard et al., 2022). Furthermore, concomitantly with the significant nitrate release, the exfoliation process resulted in the alkalinization of the water, in agreement with previous reports (Poznyak et al., 2009; Jobbágy and Regazzoni, 2011; Shafigh et al., 2019). As a matter of fact, by adding 3 g/L CaAl-LDH in water, the pH increased to 11.5. The higher availability of chlorides in the solution in contact with the particles favored the substitution mechanism, but this was a marginal effect if compared with the particle exfoliation occurring in water. In fact, the latter accounted for 75% of nitrogen release at the equilibrium, while in the case of 0.0001 mol/L NaCl, it increased to 87% of the total available. The gain grew to 96% for the 0.5 mol/L NaCl and this change was attributed to the anion exchange. Therefore, for nitrates-loaded LDH, the exfoliation was thermodynamically overwhelming.

The values of total nitrogen detected at the equilibrium for various chloride concentrations (from pure water to 0.5 M) are reported in Table 4.

Given the presence of two substitution processes, related to water molecules and chloride ions, and assuming that they were independent from each other, it was possible to highlight the anion exchange kinetic contribution by subtracting the release curves obtained in the presence of chloride and the one obtained in pure water. Results are shown in Fig. 5b, where the fraction exchanged with chlorides is reported in terms of the percentage value of the total nitrates available in the pigments (116.8 ppm). The nitrate release kinetics presented a fast development in the first 5 h, likely due to the high concentration gradient of chlorides (Brahma and Saikia, 2022). The process slowed down with time due to the decreasing availability of vacant sites and reached the equilibrium state after 24 h. The kinetic evolution followed an exponential growth model and can be modeled also with Eq. (2) (Wilczak and Keinath, 1993; Chiron et al., 2003; Zhang et al., 2022). As discussed for the SB release, parameter A depends on the chlorides availability in the surrounding environment and the amount substituted at the equilibrium. It passed from 47.8% to 82.7% increasing the Cl^- concentration from 0.0001 mol/L to 0.5 M. Furthermore, the kinetic constant k of the nitrate exchange with chloride was calculated to be $k_{avg} = 0.2 \pm 0.1\ h^{-1}$ and it was significatively lower than the k of the exfoliation process (7.4 h^{-1}). These values indicated that the exfoliation process in water was the dominant one with respect to the anion exchange process also from a kinetic point of view.

Using SB as the intercalating ion strongly stabilized the LDH structure compared with the case where nitrate ions were present in the LDH structure. In water, there was no detection of SB release, but in the

Table 4
Total nitrogen release at the equilibrium plateau at various chloride concentrations.

Cl^- conc. (mol/L)	Total nitrogen (ppm N)
Blank – pure water	88.11
0.0001	102.0
0.001	103.6
0.01	108.9
0.5	112.4

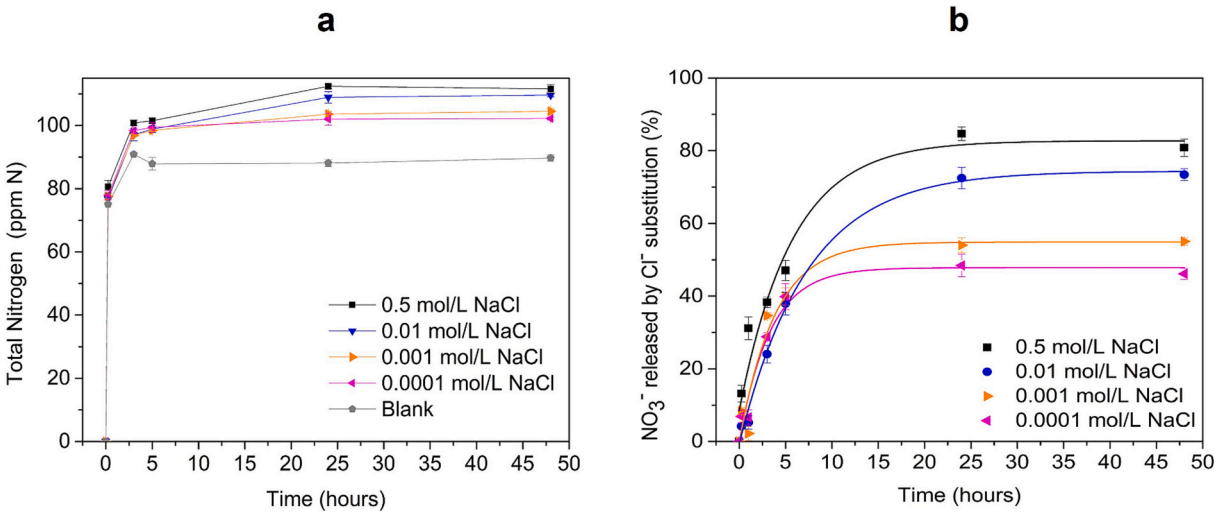

Fig. 5. Total nitrogen measurements results from pristine LDH particles immersion in 0.5 M, 0.1 M, 0.05 M, 0.01 mol/L NaCl, and pure water (Blank) solutions over contact time (a), and curves representing the fraction of the nitrates released by anion exchange (b) obtained subtracting the contribution of exfoliation (Blank).

presence of chlorides in the solution, SB substitution took place rapidly, reaching an equilibrium extent of 86.7%. Notably, when nitrate ions were the intercalating ions, the exfoliation process was the dominant one with respect to the chloride substitution both from a thermodynamic and kinetic point of view. In fact, it accounted for 75% of the anions available with a higher kinetic constant.

This rationale supported the decision to introduce SB directly during the LDH synthesis rather than opting for a subsequent ionic exchange stage. The avoidance of such sequential procedures was underpinned by the noted inadequate stability of pristine LDH particles in aqueous environments, especially when not stabilized by larger organic molecules. Consequently, there exists a potential risk that the intercalation process may jeopardize the structural integrity of LDH in the final product. Furthermore, the efficiency of such a process might be compromised given the LDH's limited inclination to exchange larger molecules, such as SB, with smaller counterparts like carbonates or nitrates.

3.3. Electrochemical characterization

The effect of each type of pigment was first evaluated through PDP and EIS to study the effect of the modified LDH on the mitigation of carbon steel corrosion. In particular, the investigated pigments were added to a neutral saline solution. To better understand the various contributions produced by SB and LDH, the curves recorded by adding the pristine SB are also shown. Furthermore, the measurements of bare carbon steel surface in the non-modified saline solution are presented as a reference, as well as that obtained in an alkalinized electrolyte produced by the addition of NaOH to reach pH 11.5, a pH condition similar to the alkalinity level provided by the addition of 3 g/L of LDH and a relevant contribution of corrosion protection in the case of steel substrates.

Fig. 6 illustrates the PDP curves obtained in the various electrolyte solutions while keeping the bare carbon steel substrate equal. The effect of SB stood out for its capability to shift the behavior of the steel to a significatively nobler (+ 0.390 *V*) open circuit potential (OCP) value. A minor rise in OCP was also evident with the LDH/SB pigments, attributable to the SB release. The presence of the inhibitor (by itself or embedded in the CaAl-LDH) promoted a shift of the anodic current densities toward smaller values. On the other hand, the effect of alkalinization of the solution given by the LDH dissolution induced the formation of a passivating environment for mild steel, enhancing the corrosion resistance with respect to the reference sample at neutral pH.

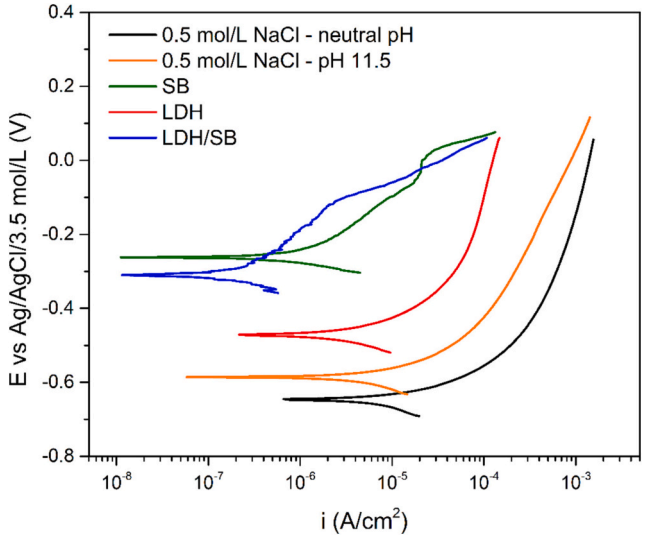

Fig. 6. Anodic polarization curves recorded after 2 h of immersion in 0.05 mol/L NaCl solution collected on bare steel surfaces where 3 g/L of pigments were added.

This fact was substantiated by the characteristics of the curve observed in the NaOH-alkalinized solution, closely resembling the LDH case. The additional shift toward lower current density could be attributed to the chloride trapping the LDH and the competitive adsorption behavior of nitrates against Cl^- ions on the metal surface (Xu et al., 2023). Furthermore, nitrate anions are known as anodic corrosion inhibitors thanks to the tendency to be reduced into nitrites in alkaline environments to promote the formation of a more stable passive film based on ferric instead of ferrous iron (Söylev and Richardson, 2008; Valcarce and Vázquez, 2008; Zuo et al., 2019). On the other hand, the inhibition effect of SB was related to the formation of a dicarboxylate complex on the metallic surface once the corrosion started and triggered the release of ferrous ions (Lahem et al., 2012). These inhibitive contributions came together to the passivation effect of the LDH dissolution resulting in the overall enhancement in the electrochemical resistance.

EIS modulus and phase spectra are given in Fig. 7a. According to the PDP outcomes, the SB was effective both as a self-standing pigment and inside the LDH (LDH/SB). The impedance modulus at low frequencies for these two samples reached higher values than for the bare substrate (Fig. 7a). The spectra were characterized by a single capacitive loop (Fig. 7b) at middle-low frequencies. The EIS raw data sets were modeled using a nonlinear least-squares fit technique, employing ZSIMPWIN® software. The analysis aimed to obtain the polarization resistance value (R_p) because it is recognized as an index of inhibition efficiency. R_p was determined from the spectra fitting exploiting an R(QR) equivalent electric circuit, where a constant phase element (CPE, namely *Q*) was employed to account for deviation from the ideal behavior. The impedance of a CPE could be expressed by Eq. (5):

$$Z_{CPE}(\omega) = [Y_0(j\omega)^n]^{-1} \quad (5)$$

where Y_0 represents the admittance constant of the CPE, n is the exponent of the CPE (ranging from −1 to 1), and ω is the angular frequency. The inhibitor efficiencies were calculated following Eq. (6) (Cao et al., 2017; Javadian et al., 2017; Nguyen et al., 2018), where R_{p0} is the polarization resistance in the case of neutral electrolytes and the absence of pigments. Since R_p represents the interfacial charge transfer process, it reflects the effectiveness of the inhibitive layer formed on the steel surface (Zuo et al., 2019).

$$IE\% = \left(R_p - R_{p0}\right)/R_p \quad (6)$$

The polarization resistance shown in Table 5 was improved already by the more alkaline pH, and its value turned out to be similar to that encountered for the LDH in the solution (7.93×10^3 Ω·cm^2). In the presence of SB, this parameter significantly changed, increasing by about one order of magnitude (8.74×10^4 Ω·cm^2). This variation of polarization resistance due to SB presence was in agreement with the data available in the literature (Lahem et al., 2012; Nguyen et al., 2018; Xu et al., 2018).

The inhibition efficiency extracted from EIS data was in accordance with the PDP outcomes since the LDH turned out to be able to enhance the corrosion resistance of carbon steel thanks to the alkalinization effect (*IE*% = 84), and the presence of SB remarkably improves the corrosion inhibition given by LDH (*IE*% = 99). The extent of the corrosion protection gain seemed to be similar in the loaded particles and the standalone SB.

The SVET analysis results supported the PDP and EIS findings, despite the lower concentration of chloride ions present in the solution in contact with the steel surface (5 times less concentrated than the previous measurements due to experimental constraints in the case of SVET that require a lower solution conductivity for enhanced resolution (Bastos et al., 2017; Izquierdo et al., 2012; Bastos et al., 2005; Cristoforetti et al., 2024)). Hence, since with 0.01 mol/L chlorides solution only 6% of SB was found to be released (as obtained from TOC analysis) and increasing the concentration up to 0.05 mol/L the released rate reaches 20%, a milder beneficial effect could be expected in the case of

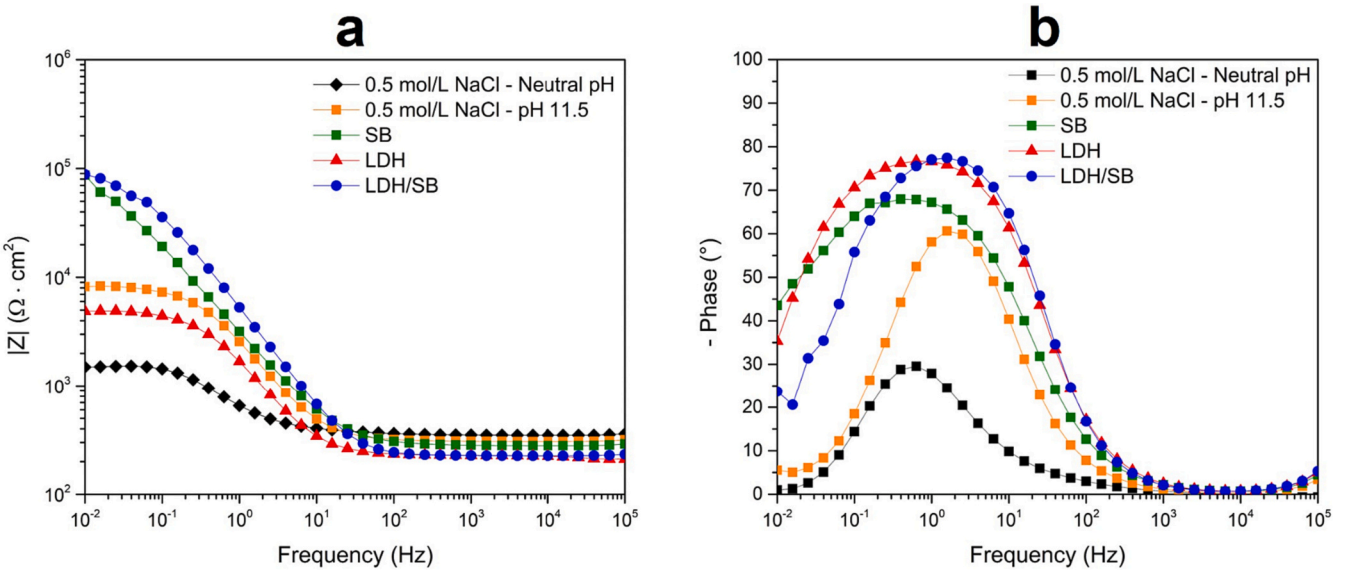

Fig. 7. Bode representation of the EIS spectra collected on a bare steel surface in 0.05 mol/L NaCl solution without and with 3 g/L of pigments in solution.

Table 5
Results for EIS data fitting using the electrochemical equivalent circuit R(QR).

Sample and condition	R_P ($\Omega \cdot cm^2$)	Y_0 ($S \cdot cm^{-2} \cdot s^n$)	n	R_{el} ($\Omega \cdot cm^2$)	IE %
0.5 mol/L NaCl – Neutral pH	1.24×10^3	4.91×10^{-4}	$8.05E \times 10^{-1}$	3.59×10^2	–
0.5 mol/L NaCl - pH 11.5	7.98×10^3	7.15×10^{-5}	9.07×10^{-1}	3.16×10^2	84
SB	1.44×10^5	7.39×10^{-5}	8.12×10^{-1}	$2.89E \times 10^2$	99
LDH	7.93×10^3	1.40×10^{-4}	8.17×10^{-1}	2.10×10^2	84
LDH/SB	8.78×10^4	3.57×10^{-5}	9.20×10^{-1}	2.32×10^2	99

the LDH/SB pigments with respect the observations from the conventional electrochemical characterization by EIS and PDP. However, this effect could be partially compensated by the less corrosive aggressivity of the more diluted saline solution employed in the SVET measurements. However, in the case of LDH loaded with nitrates, this effect was expected to be negligible, as TN data indicated that the improvement in anion exchange was <3% when transitioning from 0.01 mol/L to 0.5 M. Following a 3-h exposure to the blank saline solution, the steel surface exhibited increased electrochemical activity, both in terms of the magnitude of ionic current and the broader expansion of anodic regions (Fig. 8a). The corrosive behavior sensed by SVET appeared as a distribution of positive ionic currents, corresponding to iron ions released from the sample caused by anodic reactions, whereas the cathodic activity was related to the reduction of dissolved oxygen (Bastos et al., 2017). No preferential site for anodic or cathodic location was recognized during the measurements, thus suggesting a random distribution of the reactive regions on the bare steel surface.

As experienced in the EIS and PDP analysis, the alkaline pH of 11.5 contributed a passivating effect to the steel substrate (Fig. 8b), and the average electrochemical activity was comparable with the action produced by the dissolution of the nitrate-doped LDH (Fig. 8d). The influence of the disodium sebacate turned out to be the most efficient in the mitigation of corrosion development (Fig. 8c) thanks to the higher concentration of inhibitor, almost doubled with respect to the content loaded in the LDH/SB particles, which improved the corrosion resistance of the substrate compared to the pristine LDH (Fig. 8e).

4. Conclusions

In this study, CaAl-LDH were successfully synthesized and loaded with SB using an environmentally friendly and cost-effective hydrothermal method. The presence of the corrosion inhibitor within the hydrotalcite-like lamellar structure was confirmed through XRD and FTIR. The SB content in the pigments was estimated to be 49.2% by weight, with some remaining nitrates still partially present. Both LDH and LDH/SB configurations exhibited a natural affinity for chloride ions via an anion exchange mechanism, resulting in a maximum SB release efficiency of 86.7% by weight. The SB release and concurrent chloride ion adsorption followed a Langmuir-type isotherm. LDH intercalated with SB displayed increased stability during immersion. The release of nitrates stemmed from a combination of anion exchange with chloride ions and particle dissolution, a kinetically and thermodynamically favored process that led to liquid alkalinization. In both cases, higher chloride availability facilitated anion exchange, both kinetically and thermodynamically. Electrochemical characterization demonstrated the favorable impact of alkalinization due to LDH dissolution on the corrosion protection of carbon steel. Additionally, the known inhibitory effect of disodium sebacate was found to be effective when incorporated as an anion within the hydrotalcite-like layers. Potentiodynamic measurements, electrochemical impedance spectroscopy, and scanning vibrating electrode technique results were consistent with one another. Specifically, a more alkaline pH, combined with the inhibition effect of disodium sebacate adsorbed on the steel surface, led to a reduction in the corrosion current and an enhancement of the overall impedance of the steel surface. When compared to the pristine reference surface, the bare metal exposed to LDH doped with SB exhibited greater durability. In terms of inhibition efficiency, LDH particles loaded with SB demonstrated 99% effectiveness, compared to 84% for nitrate-containing LDH. SB intercalation resulted in improved inhibition performance and higher particle stability.

This study underscored the significant potential of anionic clays for corrosion protection of metallic structures and contributed valuable insights to the understanding of CaAl-LDH as smart nanocontainers. Further research efforts should be directed toward assessing their efficacy as pigments in protective coatings for steel substrates.

CRediT authorship contribution statement

Andrea Cristoforetti: Writing – review & editing, Writing – original

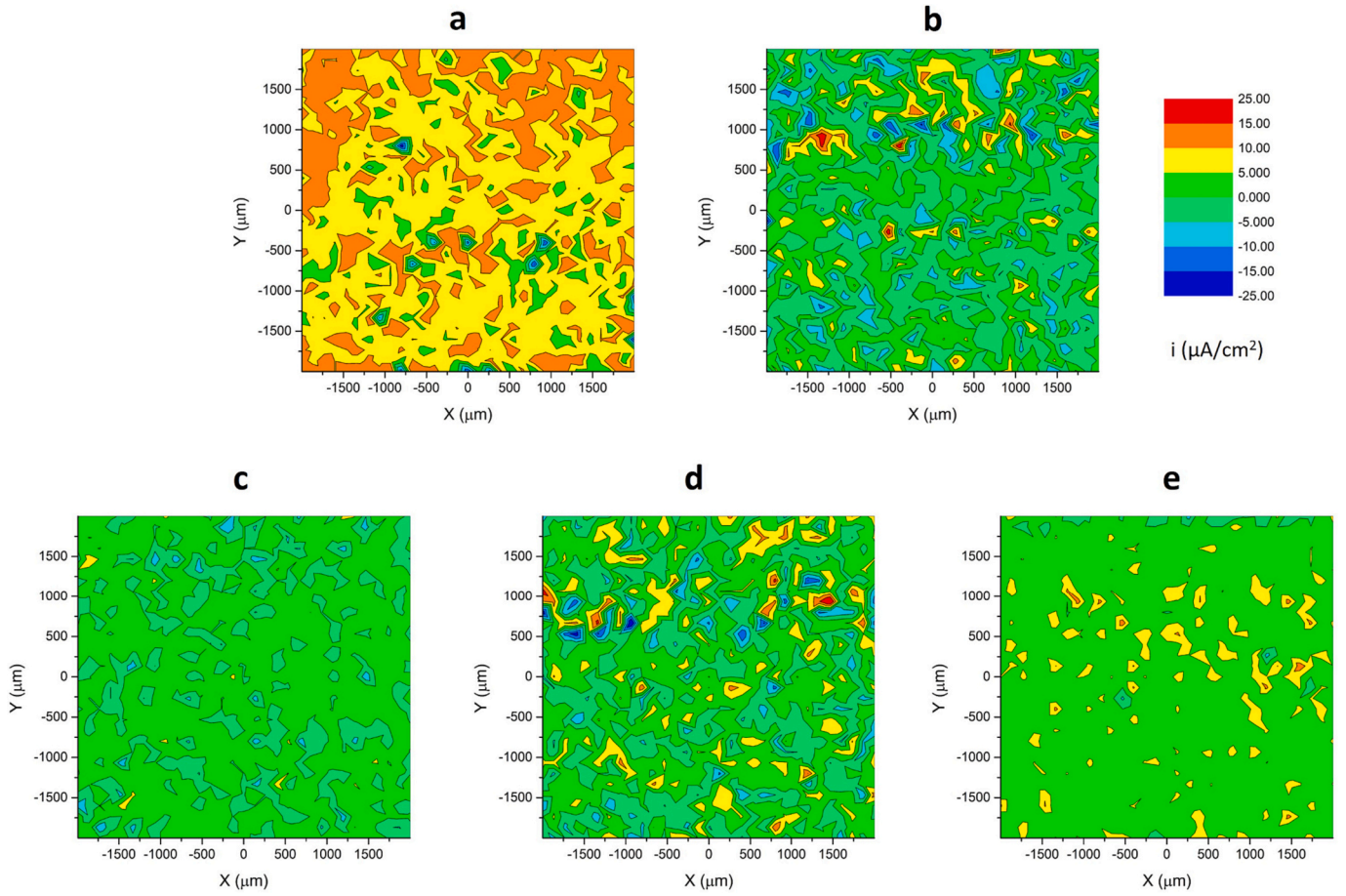

Fig. 8. Ionic current maps obtained by *SVET* on bare steel after 3 h of immersion in blank 0.01 mol/L NaCl solution (a), 0.01 mol/L NaCl alkalinized to pH 11.5 by NaOH (b), and 0.01 mol/L NaCl loaded with 3 g/L of SB (c), LDH (d), LDH/SB (e) respectively.

draft, Methodology, Investigation, Formal analysis, Data curation. **Federico Parola:** Investigation. **Francesco Parrino:** Writing – review & editing, Methodology, Formal analysis, Data curation, Conceptualization. **Javier Izquierdo:** Software, Investigation. **Ricardo M. Souto:** Writing – review & editing, Validation, Supervision, Resources, Methodology, Funding acquisition. **Stefano Rossi:** Writing – review & editing, Supervision, Project administration, Conceptualization. **Flavio Deflorian:** Supervision, Project administration. **Michele Fedel:** Writing – review & editing, Validation, Supervision, Project administration, Methodology, Conceptualization.

Declaration of competing interest

The authors declare no financial or commercial conflict of interest.

Data availability

The raw/processed data required to reproduce these findings cannot be shared at this time due to technical or time limitations.

Acknowledgments

R.M.S. and J.I. acknowledge funding by the Spanish Ministry of Science and Innovation (MICINN, Madrid, Spain), and the European Regional Development Fund (Brussels, Belgium) MCIN/AEI/10.13039/501100011033/FEDER, UE under grant PID2021-127445NB-I00.

References

Abdolmohammad-Zadeh, H., Kohansal, S., 2012. Determination of mesalamine by spectrofluorometry in human serum after solid-phase extraction with Ni-Al layered double hydroxide as a nanosorbent. J. Braz. Chem. Soc. 23, 473–481. https://doi.org/10.1590/S0103-50532012000300014.

Alibakhshi, E., Ghasemi, E., Mahdavian, M., 2014. Sodium zinc phosphate as a corrosion inhibitive pigment. Prog. Org. Coat. 77, 1155–1162. https://doi.org/10.1016/j.porgcoat.2014.03.027.

Allada, R.K., Navrotsky, A., Berbeco, H.T., Casey, W.H., 2002. Thermochemistry and aqueous solubilities of hydrotalcite-like solids. Science 296, 721–723. https://doi.org/10.1126/science.1069797.

Bastos, A.C., Ferreira, M.G.S., Simões, A.M., 2005. Comparative electrochemical studies of zinc chromate and zinc phosphate as corrosion inhibitors for zinc. Prog. Org. Coat. 52, 339–350. https://doi.org/10.1016/j.porgcoat.2004.09.009.

Bastos, A.C., Ferreira, M.G., Simões, A.M., 2006. Corrosion inhibition by chromate and phosphate extracts for iron substrates studied by EIS and SVET. Corros. Sci. 48, 1500–1512. https://doi.org/10.1016/j.corsci.2005.05.021.

Bastos, A.C., Quevedo, M.C., Karavai, O.V., Ferreira, M.G.S., 2017. Review—on the application of the scanning vibrating electrode technique (SVET) to corrosion research. J. Electrochem. Soc. 164, C973–C990. https://doi.org/10.1149/2.0431714jes.

Bernard, E., Zucha, W.J., Lothenbach, B., Mäder, U., 2022. Stability of hydrotalcite (Mg-Al layered double hydroxide) in presence of different anions. Cem. Concr. Res. 152, 106674 https://doi.org/10.1016/j.cemconres.2021.106674.

Bi, X., Zhang, H., Dou, L., 2014. Layered double hydroxide-based nanocarriers for drug delivery. Pharmaceutics 6, 298–332. https://doi.org/10.3390/pharmaceutics6020298.

Boisier, G., Lamure, A., Pébère, N., Portail, N., Villatte, M., 2009. Corrosion protection of AA2024 sealed anodic layers using the hydrophobic properties of carboxylic acids. Surf. Coat. Technol. 203, 3420–3426. https://doi.org/10.1016/j.surfcoat.2009.05.008.

Bouali, A.C., Serdechnova, M., Blawert, C., Tedim, J., Ferreira, M.G.S., Zheludkevich, M. L., 2020. Layered double hydroxides (LDHs) as functional materials for the corrosion protection of aluminum alloys: a review. Appl. Mater. Today 21, 100857. https://doi.org/10.1016/j.apmt.2020.100857.

Brahma, D., Saikia, H., 2022. Synthesis of ZrO_2/MgAl-LDH composites and evaluation of its isotherm, kinetics and thermodynamic properties in the adsorption of Congo red

dye. Chem. Thermodyn. Therm. Anal. 7, 100067 https://doi.org/10.1016/j.ctta.2022.100067.
Caballero, D., Beltrán-Cobos, R., Tavares, F., Cruz-Yusta, M., Granados, L.S., Sánchez-Moreno, M., Pavlovic, I., 2022. The inhibitive effect of sebacate-modified LDH on concrete steel reinforcement corrosion. ChemEngineering 6. https://doi.org/10.3390/chemengineering6050072.
Cao, Y., Dong, S., Zheng, D., Wang, J., Zhang, X., Du, R., Song, G., Lin, C., 2017. Multifunctional inhibition based on layered double hydroxides to comprehensively control corrosion of carbon steel in concrete. Corros. Sci. 126, 166–179. https://doi.org/10.1016/j.corsci.2017.06.026.
Cao, Y., Zheng, D., Zhang, F., Pan, J., Lin, C., 2022. Layered double hydroxide (LDH) for multi-functionalized corrosion protection of metals: a review. J. Mater. Sci. Technol. 102, 232–263. https://doi.org/10.1016/J.JMST.2021.05.078.
Chen, Y., Shui, Z., Chen, W., Chen, G., 2015. Chloride binding of synthetic Ca–Al–NO_3 LDHs in hardened cement paste. Constr. Build. Mater. 93, 1051–1058. https://doi.org/10.1016/j.conbuildmat.2015.05.047.
Chiron, N., Guilet, R., Deydier, E., 2003. Adsorption of Cu(II) and Pb(II) onto a grafted silica: isotherms and kinetic models. Water Res. 37, 3079–3086. https://doi.org/10.1016/S0043-1354(03)00156-8.
Choy, J.H., Kim, Y.K., Son, Y.H., Choy, Y.B., Oh, J.M., Jung, H., Hwang, S.J., 2008. Nanohybrids of edible dyes intercalated in ZnAl layered double hydroxides. J. Phys. Chem. Solids 69, 1547–1551. https://doi.org/10.1016/J.JPCS.2007.11.009.
Cristoforetti, A., Fedel, M., Deflorian, F., Rossi, S., 2021. Influence of deposition parameters on the behavior of nitro-cobalt-based and Ti-hexafluoride-based pretreatments. J. Coat. Technol. Res. 19, 859–873. https://doi.org/10.1007/s11998-021-00563-0.
Cristoforetti, A., Izquierdo, J., Souto, R.M., Deflorian, F., Fedel, M., Rossi, S., 2024. In-situ measurement of electrochemical activity related to filiform corrosion in organic coated steel by scanning vibrating electrode technique and scanning micropotentiometry. Corros. Sci. 227, 111669 https://doi.org/10.1016/j.corsci.2023.111669.
Czakis-Sulikowska, D., Czylkowska, A., 2004. Complexes of Mn(II), Co(II), Ni(II) and Cu(II) with 4,4′-bipyridine and dichloroacetates. J. Therm. Anal. Calorim. 71, 395–405. https://doi.org/10.1023/a:1022879120867.
De Sá, F.P., Cunha, B.N., Nunes, L.M., 2013. Effect of pH on the adsorption of Sunset Yellow FCF food dye into a layered double hydroxide (CaAl-LDH-NO_3). Chem. Eng. J. 215–216, 122–127. https://doi.org/10.1016/J.CEJ.2012.11.024.
Dobson, K.D., McQuillan, A.J., 1999. In situ infrared spectroscopic analysis of the adsorption of aliphatic carboxylic acids to TiO_2, ZrO_2, Al_2O_3, and Ta_2O_5 from aqueous solutions. Spectrochim. Acta A Mol. Biomol. Spectrosc. 55, 1395–1405. https://doi.org/10.1016/S1386-1425(98)00303-5.
Dodds, P.C., Williams, G., Radcliffe, J., 2017. Chromate-free smart release corrosion inhibitive pigments containing cations. In: Progress in Organic Coatings, 6th International Conference: Advances in Corrosion Protection by Organic Coatings, 102, pp. 107–114. https://doi.org/10.1016/j.porgcoat.2016.05.005.
Dolamic, I., Bürgi, T., 2006. Photoassisted decomposition of malonic acid on TiO_2 studied by in situ attenuated total reflection infrared spectroscopy. J. Phys. Chem. B 110, 14898–14904. https://doi.org/10.1021/jp0616967.
Dolamic, I., Bürgi, T., 2007. Photocatalysis of dicarboxylic acids over TiO_2: an in situ ATR-IR study. J. Catal. 248, 268–276. https://doi.org/10.1016/j.jcat.2007.03.020.
Drits, V.A., Sokolova, T.N., Sokolova, G.V., Cherkashin, V.A., 1987. New members of the hydrotalcite-manasseite group. Clay Clay Miner. 35, 401–417. https://doi.org/10.1346/CCMN.1987.0350601.
Epp, J., 2016. 4 - X-ray diffraction (XRD) techniques for materials characterization. In: Hübschen, G., Altpeter, I., Tschuncky, R., Herrmann, H.-G. (Eds.), Materials Characterization Using Nondestructive Evaluation (NDE) Methods. Woodhead Publishing, pp. 81–124. https://doi.org/10.1016/B978-0-08-100040-3.00004-3.
Fedel, M., Zampiccoli, M., 2021. Insight into the role of cerium (III) addition to a MgAl-LDH coating on AA6082. Appl. Sci. 11, 8252. https://doi.org/10.3390/app11178252.
Fedel, M., Poelman, M., Olivier, M., Deflorian, F., 2019. Sebacic acid as corrosion inhibitor for hot-dip galvanized (HDG) steel in 0.1 M NaCl. Surf. Interface Anal. 51, 541–551. https://doi.org/10.1002/sia.6617.
Fedel, M., Zanella, C., Ferrari, L., Deflorian, F., 2021. Effect of the synthesis parameters of in situ grown Mg-Al LDHs on the filiform corrosion susceptibility of painted AA5005. Electrochim. Acta 381, 138288. https://doi.org/10.1016/J.ELECTACTA.2021.138288.
Fedel, M., Zonta, S., Cristoforetti, A., 2024. Study of ZnAl Hydroxides-Based Thin Films to Enhance the Filiform Corrosion Resistance of Acrylic-Coated AA5005. J. Electrochem. Soc. 171, 021501 https://doi.org/10.1149/1945-7111/ad2599.
Forsgren, A., 1996. Corrosion Control Through Organic Coatings, 2006. CRC press.
Georges, C., Rocca, E., Steinmetz, P., 2008. Synergistic effect of tolutriazol and sodium carboxylates on zinc corrosion in atmospheric conditions. Electrochim. Acta 53, 4839–4845. https://doi.org/10.1016/j.electacta.2008.01.073.
Godinez-Alvarez, J.M., Mora-Mendoza, J.L., Rodriguez-Betancourt, E., Zavala-Olivares, G., Gonzalez-Nunez, M.A., 2004. Inhibition of ferrous metal corrosion by carboxylates. In: Presented at the Corrosion 2004 p. NACE-04412.
Gomes, C., Mir, Z., Sampaio, R., Bastos, A., Tedim, J., Maia, F., Rocha, C., Ferreira, M., 2020. Use of ZnAl-layered double hydroxide (LDH) to extend the service life of reinforced concrete. Materials 13, 1769. https://doi.org/10.3390/ma13071769.
Grigoriev, D., 2015. Chapter 8 - intelligent coatings for corrosion control. In: Anticorrosion Coatings with Self-Recovering Ability Based on Damage-Triggered Micro- and Nanocontainers. Elsevier Inc., pp. 283–333. https://doi.org/10.1016/B978-0-12-411467-8.00008-8
Grundmeier, G., Schmidt, W., Stratmann, M., 2000. Corrosion protection by organic coatings: electrochemical mechanism and novel methods of investigation. Electrochim. Acta 45, 2515–2533. https://doi.org/10.1016/S0013-4686(00)00348-0.
Guo, Y., Jin, P., Shao, M., Dong, S., Du, R., Lin, C., 2022. Effect of an environmentally friendly diisooctyl sebacate-based mixed corrosion inhibitor on reinforcing steel. Acta Phys. -Chim. 38 https://doi.org/10.3866/PKU.WHXB202003033.
Hefter, G.T., North, N.A., Tan, S.H., 1997. Organic corrosion inhibitors in neutral solutions; part 1 — inhibition of steel, copper, and aluminum by straight chain carboxylates. Corrosion 53, 657–667. https://doi.org/10.5006/1.3290298.
Ho, Y.S., J.C.Y.N, McKay, G., 2000. Kinetics of pollutant sorption by biosorbents: review. Sep. Purif. Methods 29, 189–232. https://doi.org/10.1081/SPM-100100009.
Indumathi, S.M., Vasudevan, T., Sundarrajan, S., Subba Rao, B.V., Murthy, C.V.S., Yadav, D.R., 2011. Cadmium- and chromate-free coating schemes for corrosion protection of 15CDV6 steel. Met. Finish. 109, 15–21. https://doi.org/10.1016/S0026-0576(11)00010-9.
Izquierdo, J., Santana, J.J., González, S., Souto, R.M., 2012. Scanning microelectrochemical characterization of the anti-corrosion performance of inhibitor films formed by 2-mercaptobenzimidazole on copper. Prog. Org. Coat. 74, 526–533. https://doi.org/10.1016/j.porgcoat.2012.01.019.
Javadian, S., Darbasizadeh, B., Yousefi, A., Ektefa, F., Dalir, N., Kakemam, J., 2017. Dye-surfactant aggregates as corrosion inhibitor for mild steel in NaCl medium: experimental and theoretical studies. J. Taiwan Inst. Chem. Eng. 71, 344–354. https://doi.org/10.1016/j.jtice.2016.11.014.
Jobbágy, M., Regazzoni, A.E., 2011. Dissolution of nano-size Mg–Al–Cl hydrotalcite in aqueous media. Appl. Clay Sci. 51, 366–369. https://doi.org/10.1016/j.clay.2010.11.027.
Kalenda, P., Kalendová, A., Štengl, V., Antoš, P., Šubrt, J., Kváča, Z., Bakardjieva, S., 2004. Properties of surface-treated mica in anticorrosive coatings. Prog. Org. Coat. 49, 137–145. https://doi.org/10.1016/j.porgcoat.2003.09.003.
Kameda, T., Miyano, Y., Yoshioka, T., Uchida, M., Okuwaki, A., 2000. New treatment methods for waste water containing chloride ion using magnesium-aluminum oxide. Chem. Lett. 1136–1137. https://doi.org/10.1246/cl.2000.1136.
Kloprogge, J.T., Wharton, D., Hickey, L., Frost, R.L., 2002. Infrared and Raman study of interlayer anions CO_3^{2-}, NO_3^-, SO_4^{2-} and ClO_4^- in Mg/Al-hydrotalcite. Am. Mineral. 87, 623–629. https://doi.org/10.2138/am-2002-5-604.
Kokalj, A., 2022. On the use of the Langmuir and other adsorption isotherms in corrosion inhibition. SSRN Electron. J. 217, 111112 https://doi.org/10.2139/ssrn.4310526.
Lahem, D., Poelman, M., Atmani, F., Olivier, M.G., 2012. Synergistic improvement of inhibitive activity of dicarboxylates in preventing mild steel corrosion in neutral aqueous solution. Corros. Eng. Sci. Technol. 47, 463–471. https://doi.org/10.1179/1743278212Y.0000000030.
Lazaridis, N.K., Asouhidou, D.D., 2003. Kinetics of sorptive removal of chromium(VI) from aqueous solutions by calcined Mg–Al–CO3 hydrotalcite. Water Res. 37, 2875–2882. https://doi.org/10.1016/S0043-1354(03)00119-2.
Lewandowski, W., Kalinowska, M., Lewandowska, H., 2005. The influence of metals on the electronic system of biologically important ligands. Spectroscopic study of benzoates, salicylates, nicotinates and isoorotates. Review. J. Inorg. Biochem. 99, 1407–1423. https://doi.org/10.1016/j.jinorgbio.2005.04.010.
Li, D., Wang, F., Yu, X., Wang, J., Liu, Q., Yang, P., He, Y., Wang, Y., Zhang, M., 2011. Anticorrosion organic coating with layered double hydroxide loaded with corrosion inhibitor of tungstate. Prog. Org. Coat. 71, 302–309. https://doi.org/10.1016/j.porgcoat.2011.03.023.
Li, C., He, Y., Zhao, Y., Li, Z., Sun, D., Li, H., Chen, W., Yan, J., Wu, G., Yuan, X., 2023. Cataphoretic deposition of an epoxy coating with the incorporation of $Ti_3C_2T_x$@Mg-Al layered double hydroxide for long-term active corrosion protection effect. Prog. Org. Coat. 175, 107333 https://doi.org/10.1016/j.porgcoat.2022.107333.
Lu, Y., Miller, J.D., 2002. Carboxyl stretching vibrations of spontaneously adsorbed and LB-transferred calcium carboxylates as determined by FTIR internal reflection spectroscopy. J. Colloid Interface Sci. 256, 41–52. https://doi.org/10.1006/jcis.2001.8112.
Lv, L., He, J., Wei, M., Evans, D.G., Duan, X., 2006. Uptake of chloride ion from aqueous solution by calcined layered double hydroxides: equilibrium and kinetic studies. Water Res. 40, 735–743. https://doi.org/10.1016/j.watres.2005.11.043.
Lyon, S.B., Bingham, R., Mills, D.J., 2017. Advances in corrosion protection by organic coatings: what we know and what we would like to know. Prog. Org. Coat. 102, 2–7. https://doi.org/10.1016/j.porgcoat.2016.04.030.
Mahajanam, S.P.V., Buchheit, R.G., 2008. Characterization of inhibitor release from Zn-Al-$[V10O28]^{6-}$ hydrotalcite pigments and corrosion protection from hydrotalcite-pigmented epoxy coatings. Corrosion 64, 230–240. https://doi.org/10.5006/1.3278468.
Mahdavian, A.M., Attar, M.M., 2005. Investigation on zinc phosphate effectiveness at different pigment volume concentrations via electrochemical impedance spectroscopy. Electrochim. Acta 50, 4645–4648. https://doi.org/10.1016/j.electacta.2005.02.015.
Mei, Y., Xu, J., Jiang, L., Tan, Q., 2019. Enhancing corrosion resistance of epoxy coating on steel reinforcement by aminobenzoate intercalated layered double hydroxides. Prog. Org. Coat. 134, 288–296. https://doi.org/10.1016/j.porgcoat.2019.05.023.
Meyn, M., Beneke, K., Lagaly, G., 1990. Anion-exchange reactions of layered double hydroxides. Inorg. Chem. 29, 5201–5207. https://doi.org/10.1021/ic00351a013.
Millange, F., Walton, R.I., Lei, L., O'Hare, D., 2000. Efficient separation of terephthalate and phthalate anions by selective ion-exchange intercalation in the layered double hydroxide $Ca_2Al(OH)_6{\cdot}NO_3{\cdot}2H_2O$. Chem. Mater. 12, 1990–1994. https://doi.org/10.1021/CM0002057.
Milošev, I., Frankel, G.S., 2018. Review—conversion coatings based on zirconium and/or titanium. J. Electrochem. Soc. 165, C127–C144. https://doi.org/10.1149/2.0371803jes.

Miyata, S., 1983. Anion-exchange properties of hydrotalcite-like compounds. Clay Clay Miner. 31, 305–311. https://doi.org/10.1346/CCMN.1983.0310409.
Nara, M., Tanokura, M., 2008. Infrared spectroscopic study of the metal-coordination structures of calcium-binding proteins. Biochem. Biophys. Res. Commun. 369, 225–239. https://doi.org/10.1016/j.bbrc.2007.11.188. Ebashi Memorial Issue.
Newman, S.P., Jones, W., 1998. Synthesis, characterization and applications of layered double hydroxides containing organic guests. New J. Chem. 22, 105–115. https://doi.org/10.1039/a708319j.
Nguyen, D.T., To, H.T.X., Gervasi, J., Paint, Y., Gonon, M., Olivier, M.G., 2018. Corrosion inhibition of carbon steel by hydrotalcites modified with different organic carboxylic acids for organic coatings. Prog. Org. Coat. 124, 256–266. https://doi.org/10.1016/j.porgcoat.2017.12.006.
Pélissier, K., Thierry, D., 2020. Powder and high-solid coatings as anticorrosive solutions for marine and offshore applications? A review. Coatings 10. https://doi.org/10.3390/COATINGS10100916.
Poznyak, S.K., Tedim, J., Rodrigues, L.M., Salak, A.N., Zheludkevich, M.L., Dick, L.F.P., Ferreira, M.G.S., 2009. Novel inorganic host layered double hydroxides intercalated with guest organic inhibitors for anticorrosion applications. ACS Appl. Mater. Interfaces 1, 2353–2362. https://doi.org/10.1021/am900495r.
Prosek, T., Thierry, D., 2004. A model for the release of chromate from organic coatings. Prog. Org. Coat. 49, 209–217. https://doi.org/10.1016/j.porgcoat.2003.09.012.
Radha, A., Kamath, P.V., Shivakumara, C., 2005. Mechanism of the anion exchange reactions of the layered double hydroxides (LDHs) of Ca and Mg with Al. Solid State Sci. 7, 1180–1187.
Rammelt, U., Köhler, S., Reinhard, G., 2008. EIS characterization of the inhibition of mild steel corrosion with carboxylates in neutral aqueous solution. Electrochim. Acta 53, 6968–6972. https://doi.org/10.1016/j.electacta.2008.01.004.
Rammelt, U., Koehler, S., Reinhard, G., 2011. Electrochemical characterisation of the ability of dicarboxylic acid salts to the corrosion inhibition of mild steel in aqueous solutions. Corros. Sci. 53, 3515–3520. https://doi.org/10.1016/j.corsci.2011.06.023.
Rocca, E., Steinmetz, J., 2001. Inhibition of lead corrosion with saturated linear aliphatic chain monocarboxylates of sodium. Corros. Sci. 43, 891–902. https://doi.org/10.1016/S0010-938X(00)00115-3.
Saha, S., Ray, S., Ghosh, S., Chakraborty, J., 2018. pH-dependent facile synthesis of CaAl-layered double hydroxides and its effect on the growth inhibition of cancer cells. J. Am. Ceram. Soc. 101, 3924–3935. https://doi.org/10.1111/jace.15555.
Saurbier, K., Schultze, J.W., Geke, J., 1994. Temporary inhibitors of corrosion in wet atmosphere: electrochemical investigations of the mechanism and efficiency. Electrochim. Acta 39, 1171–1178. https://doi.org/10.1016/0013-4686(94)E0033-V.
Shafigh, M., Hamidpour, M., Furrer, G., 2019. Zinc release from Zn-Mg-Fe(III)-LDH intercalated with nitrate, phosphate and carbonate: the effects of low molecular weight organic acids. Appl. Clay Sci. 170, 135–142. https://doi.org/10.1016/j.clay.2019.01.016.
Shulman, G.P., Bauman, A.J., 1995. Organic acid sealants for anodized aluminum—a new method for corrosion protection. Met. Finish. 93, 16–19. https://doi.org/10.1016/0026-0576(95)91305-7.
Sinko, J., 2001. Challenges of chromate inhibitor pigments replacement in organic coatings. Prog. Org. Coat. 42, 267–282. https://doi.org/10.1016/S0300-9440(01)00202-8.
Söylev, T.A., Richardson, M.G., 2008. Corrosion inhibitors for steel in concrete: state-of-the-art report. Constr. Build. Mater. 22, 609–622. https://doi.org/10.1016/j.conbuildmat.2006.10.013.
Stimpfling, T., Leroux, F., Hintze-Bruening, H., 2014. Organo-modified layered double hydroxide in coating formulation to protect AA2024 from corrosion. Colloids Surf. A Physicochem. Eng. Asp. 458, 147–154. https://doi.org/10.1016/j.colsurfa.2014.01.042.
Szabados, M., Mészáros, R., Erdei, S., Kónya, Z., Kukovecz, Á., Sipos, P., Pálinkó, I., 2016. Ultrasonically-enhanced mechanochemical synthesis of CaAl-layered double hydroxides intercalated by a variety of inorganic anions. Ultrason. Sonochem. 31, 409–416. https://doi.org/10.1016/j.ultsonch.2016.01.026.
Tabish, M., Zhao, J., Wang, J., Anjum, M.J., Qiang, Y., Yang, Q., Mushtaq, M.A., Yasin, G., 2022. Improving the corrosion protection ability of epoxy coating using CaAl LDH intercalated with 2-mercaptobenzothiazole as a pigment on steel substrate. Prog. Org. Coat. 165, 106765 https://doi.org/10.1016/j.porgcoat.2022.106765.
Tedim, J., Kuznetsova, A., Salak, A.N., Montemor, F., Snihirova, D., Pilz, M., Zheludkevich, M.L., Ferreira, M.G.S., 2012. Zn–Al layered double hydroxides as chloride nanotraps in active protective coatings. Corros. Sci. 55, 1–4. https://doi.org/10.1016/j.corsci.2011.10.003.
Trentin, A., Pakseresht, A., Duran, A., Castro, Y., Galusek, D., 2022. Electrochemical characterization of polymeric coatings for corrosion protection: a review of advances and perspectives. Polymers 14, 2306. https://doi.org/10.3390/polym14122306.
Valcarce, M.B., Vázquez, M., 2008. Carbon steel passivity examined in alkaline solutions: the effect of chloride and nitrite ions. Electrochim. Acta 53, 5007–5015. https://doi.org/10.1016/j.electacta.2008.01.091.
Van Den Brand, J., Blajiev, O., Beentjes, P.C.J., Terryn, H., De Wit, J.H.W., 2004. Interaction of anhydride and carboxylic acid compounds with aluminum oxide surfaces studied using infrared reflection absorption spectroscopy. Langmuir 20, 6308–6317. https://doi.org/10.1021/la0496845.
Vargová, Z., Almáši, M., Arabuli, L., Györyová, K., Zeleňák, V., Kuchár, J., 2011. Utilization of IR spectral detailed analysis for coordination mode determination in novel Zn-cyclen-aminoacid complexes. Spectrochim. Acta A Mol. Biomol. Spectrosc. 78, 788–793. https://doi.org/10.1016/j.saa.2010.12.022.
Vieille, L., Rousselot, I., Leroux, F., Besse, J.-P., Taviot-Guého, C., 2003. Hydrocalumite and its polymer derivatives. 1. Reversible thermal behavior of Friedel's salt: a direct observation by means of high-temperature in situ powder X-ray diffraction. Chem. Mater. 15, 4361–4368. https://doi.org/10.1021/cm031069j.
Wang, J., Guo, X., 2020. Adsorption isotherm models: classification, physical meaning, application and solving method. Chemosphere 258, 127279. https://doi.org/10.1016/j.chemosphere.2020.127279.
Wilczak, A., Keinath, T.M., 1993. Kinetics of sorption and desorption of copper(II) and lead (II) on activated carbon. Water Environ. Res. 65, 238–244. https://doi.org/10.2175/WER.65.3.7.
Williams, G., 2010. Critical factors in the inhibition of filiform corrosion by in-coating ion-exchange pigments. ECS Trans. 24, 67–76. https://doi.org/10.1149/1.3453607.
Williams, G., McMurray, H.N., 2012. Inhibition of filiform corrosion on organic-coated AA2024-T3 by smart-release cation and anion-exchange pigments. Electrochim. Acta 69, 287–294. https://doi.org/10.1016/j.electacta.2012.03.002.
Wint, N., Eaves, D., Williams, G., McMurray, H.N., 2021. The use of anion exchange pigments to inhibit the filiform corrosion of zinc-aluminium-magnesium coated steel. Corros. Sci. 193, 109886 https://doi.org/10.1016/J.CORSCI.2021.109886.
Xu, J., Song, Y., Tan, Q., Jiang, L., 2017. Chloride absorption by nitrate, nitrite and aminobenzoate intercalated layered double hydroxides. J. Mater. Sci. 52, 5908–5916. https://doi.org/10.1007/s10853-017-0826-y.
Xu, J., Song, Y., Zhao, Y., Jiang, L., Mei, Y., Chen, P., 2018. Chloride removal and corrosion inhibitions of nitrate, nitrite-intercalated Mg Al layered double hydroxides on steel in saturated calcium hydroxide solution. Appl. Clay Sci. 163, 129–136. https://doi.org/10.1016/j.clay.2018.07.023.
Xu, Z., Wu, Y., Zhang, Zhangmin, Wang, Y., Hu, J., Ma, Y., Zhang, Zuhua, Huang, H., Wei, J., Yu, Q., Shi, C., 2023. A review on the research progress of LDHs as corrosion inhibitors for reinforced concrete. J. Build. Eng. 70, 106303 https://doi.org/10.1016/j.jobe.2023.106303.
Zeleňák, V., Vargová, Z., Györyová, K., 2007. Correlation of infrared spectra of zinc(II) carboxylates with their structures. Spectrochim. Acta A Mol. Biomol. Spectrosc. 66, 262–272. https://doi.org/10.1016/j.saa.2006.02.050.
Zhang, P., Qian, G., Xu, Z.P., Shi, H., Ruan, X., Yang, J., Frost, R.L., 2012. Effective adsorption of sodium dodecylsulfate (SDS) by hydrocalumite (CaAl-LDH-Cl) induced by self-dissolution and re-precipitation mechanism. J. Colloid Interface Sci. 367, 264–271. https://doi.org/10.1016/J.JCIS.2011.10.036.
Zhang, Q., Ji, F., Jiang, L., Shen, Q., Mao, Y., Liu, C., 2022. Glycine-and alanine-intercalated layered double hydroxides as highly efficient adsorbents for phosphate with kinetic advantages. Nanomaterials 12. https://doi.org/10.3390/nano12040586.
Zheludkevich, M.L., Poznyak, S.K., Rodrigues, L.M., Raps, D., Hack, T., Dick, L.F., Nunes, T., Ferreira, M.G.S., 2010. Active protection coatings with layered double hydroxide nanocontainers of corrosion inhibitor. Corros. Sci. 52, 602–611. https://doi.org/10.1016/j.corsci.2009.10.020.
Zheludkevich, M.L., Tedim, J., Ferreira, M.G.S., 2012. "Smart" coatings for active corrosion protection based on multi-functional micro and nanocontainers. Electrochim. Acta 82, 314–323. https://doi.org/10.1016/J.ELECTACTA.2012.04.095.
Zuo, J., Wu, B., Luo, C., Dong, B., Xing, F., 2019. Preparation of MgAl layered double hydroxides intercalated with nitrite ions and corrosion protection of steel bars in simulated carbonated concrete pore solution. Corros. Sci. 152, 120–129. https://doi.org/10.1016/j.corsci.2019.03.007.